ACS APPLIED MATERIALS & INTERFACES

Research Article

www.acsami.org

Enhancing Mechanical Properties of Highly Efficient Polymer Solar Cells Using Size-Tuned Polymer Nanoparticles

Dong Jin Kang,[†] Han-Hee Cho,[†] Inhwa Lee,[‡] Ki-Hyun Kim,[†] Hyeong Jun Kim,[†] Kin Liao,[§] Taek-Soo Kim,[‡] and Bumjoon J. Kim*[,†]

[†]Department of Chemical and Biomolecular Engineering, Korea Advanced Institute of Science and Technology (KAIST), Daejeon 305-701, Republic of Korea

[‡]Department of Mechanical Engineering, Korea Advanced Institute of Science and Technology (KAIST), Daejeon 305-701, Republic of Korea

[§]Department of Mechanical Engineering, Khalifa University, Abu Dhabi, United Arab Emirates

Supporting Information

ABSTRACT: The low mechanical durability of polymer solar cells (PSCs) has been considered as one of the critical hurdles for their commercialization. We described a facile and powerful strategy for enhancing the mechanical properties of PSCs while maintaining their high power conversion efficiency (PCE) by using monodispersed polystyrene nanoparticles (PS NPs). We prepared highly monodispersed, size-controlled PS NPs (60, 80, and 100 nm), and used them to modify the poly(3,4-ethylenedioxythiophene):poly(styrenesulfonate) (PEDOT:PSS) anode buffer layer (ABL). The PS NPs played two important roles; i.e., they served as (1) binders in the PEDOT:PSS films, and (2) interfacial modifiers between ABL and the active layer, resulting in remarkable improvement of the mechanical integrity of the PSCs. The addition of PS NPs enhanced the inherent mechanical toughness of the PEDOT:PSS ABL due to their elastic properties, allowing the modified ABL to tolerate higher mechanical deformations. In addition, the adhesion energy (G_c) between the active layer and the modified PEDOT:PSS layer was enhanced significantly, i.e., by a factor of more than 1.5. The G_c value has a strong relationship with the sizes of the PS NP, showing the greatest enhancement when the largest size PS NPs (100 nm) were used. In addition, PS NPs significantly improve the air-stability of the PSCs by suppressing moisture adsorption and corrosion of the electrodes. Thus, the modification of ABL with PS NPs effectively enhances both the mechanical and the long-term stabilities of the PSCs without sacrificing their PCE values, demonstrating their great potential as applications in flexible organic electronics.

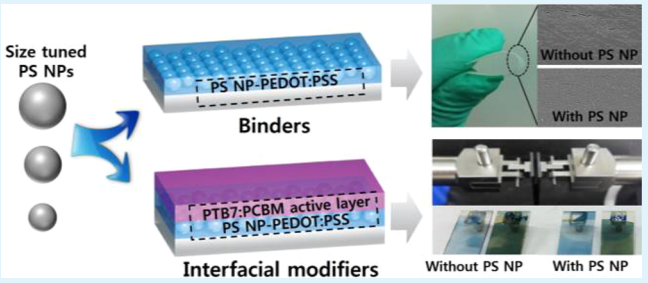

KEYWORDS: *polymer nanoparticles, PEDOT:PSS, anode buffer layer, mechanical properties, polymer solar cell*

INTRODUCTION

Polymer solar cells (PSCs) have attracted significant attention because of their various advantages, such as light weight, flexibility, and low cost.[1−5] Recently, numerous efforts have been made to enhance the performance of the PSCs, and their power conversion efficiency (PCE) has been increased rapidly to 8−9%.[6−12] However, conjugated polymers typically have much lower mechanical strength compared to their metal counterparts as well as general engineering plastics. Therefore, the PSCs made of conjugated polymer layers have a low mechanical integrity, associated with adhesive and cohesive debonding of the layers.[13] In particular, the weak interfacial adhesion of the multilayered PSCs causes low processing yields and poor stabilities of the PSCs, resulting in their degradation during subsequent operation.[13−15] Considering the potential applications of the PSCs as printable and portable devices on a flexible substrate, the weak mechanical integrity of the PSCs must be addressed. However, despite such importance, the research progress related to enhancing the mechanical properties of PSCs has been minimal compared to the progress in improving their PCE numbers.[16−18]

While poly(3,4-ethylenedioxythiophene):poly(styrenesulfonate) (PEDOT:PSS) film is the most widely used anode buffer layer (ABL) in high performance PSCs due to its high electrical conductivity and water solubility,[19] there are a number of challenges that should be overcome including strong acidity, brittleness, instability of its conductance, and reduced conductivity at large strains.[20−22] From a mechanical perspective, the interface of the hydrophobic active layer and the hydrophilic PEDOT:PSS film was typically the weakest point among the relevant layers in the PSCs, so that two layers can be easily delaminated even with small applied stress.[23−26] For example,

Received: November 5, 2014
Accepted: January 14, 2015
Published: January 14, 2015

DOI: 10.1021/am507710p
ACS Appl. Mater. Interfaces 2015, 7, 2668−2676

Scheme 1. Schematic Illustration of Different Sizes of PS NPs and Their Applications in the Modification of the PEDOT:PSS Film: (a) PS NPs as Binders in the PEDOT:PSS Polymers, and (b) PS NPs as Interfacial Modifers between PEDOT:PSS and Active Layer

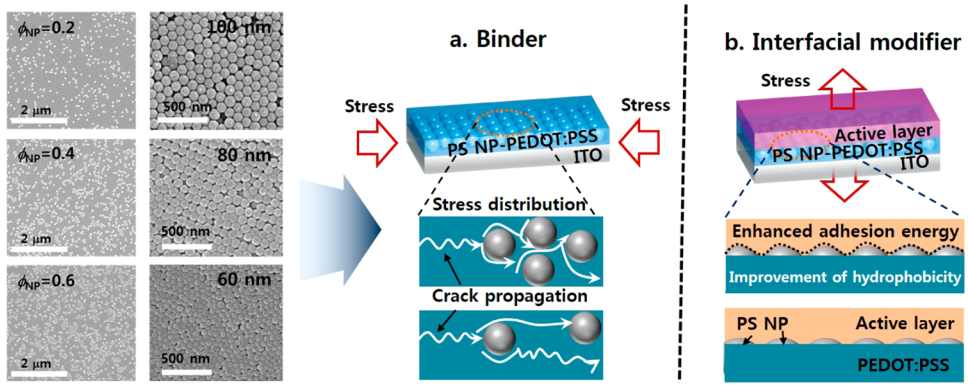

the poly(3-hexylthiophene):phenyl C_{61}-butyric acid methyl ester (PCBM) and PEDOT:PSS films had a very low adhesion energy of only ~1.5 J m^{-2}.[27] Furthermore, the PEDOT:PSS produces acidic and hygroscopic environments that accelerate the degradation of PSCs.[28−31] To alleviate these problems, the PEDOT:PSS films have been modified with interfacial modifiers, such as surfactants and self-assembled monolayers.[32−37] However, none of the previous works have focused on the effect of the modification of the PEDOT:PSS ABL on the mechanical durability of the PSCs.[38−40]

In this paper, we developed a series of cross-linked, monodispersed polystyrene nanoparticles (PS NPs) with three different sizes of 60, 80, and 100 nm that were used for modifying the PEDOT:PSS ABL. A systematic study of their effects on the mechanical and electrical properties of the ABL film as well as the characteristics and stabilities of the PSCs was described as a function of the size and volume fraction (ϕ_{NP}) of PS NPs (Scheme 1). The PS NPs have two major roles to enhance the mechanical properties of the PSCs. First, the fracture toughness and tensile strength of the pristine PEDOT:PSS could be remarkably improved due to the interlocking force between the PEDOT:PSS domains by the PS NPs acting as "binders". Second, the PS NPs can be used as "interfacial modifiers" between the hydrophilic PEDOT:PSS ABL and the hydrophobic active layer. For example, the adhesion energy (G_c) between the ABL and the active layer was dramatically improved with addition of the PS NPs. Interestingly, the interfacial property between PEDOT:PSS and the active layer was more strongly dependent on the size of the PS NPs than on the ϕ_{NP} value. In addition, the PS NPs in the PEDOT:PSS film could effectively suppress the moisture adsorption and the corrosion of ITO cathode. Therefore, we demonstrated highly efficient PSCs exceeding 7.5% PCE value while simultaneously enhancing their mechanical properties and long-term stabilities.

EXPERIMENTAL SECTION

Materials. Commercially available PEDOT:PSS (PH500), poly-[[4,8-bis[(2-ethylhexyl)oxy]benzo[1,2-b:4,5- b′]dithiophene-2,6-diyl]-[3-fluoro-2-[(2-ethylhexyl)carbonyl]thieno[3,4-]thiophenediyl]] (PTB7), and phenyl C_{71}-butyric acid methyl ester ($PC_{71}BM$) were purchased from BASF, 1-material, and Nano-C, respectively.

Synthesis of Three Different Sizes of PS NPs. Styrene was purified with an aluminum oxide column. The other organic reagents were used without further purification, which included poly(vinyl-pyrrolidone) (PVP) (M_w = 55 000 g/mol), divinylbenzene (DVB), and 2,2-azobis(2-methylpropionamidine) (AIBA). The different concentrations of PVP, DVB, and styrene monomer were carried out in a deionized water in a 200 mL, two-neck flask and was stirred at 50 °C. After 30 min of stirring, AIBA was added to the solution. The reaction temperature was gradually increased to 70 °C. After heating for 24 h at 70 °C, the mixture was cooled down to room temperature. The resultant PS NPs were filtered and repeatedly washed by being centrifuged in deionized water and methanol to remove the residual styrene and PVP. The samples were dried in a vacuum oven at 50 °C for 12 h. The size and size distribution of the PS NPs were measured using a Hitachi S-4800 scanning electron microscope. The three different sizes of PS NPs were determined to have average diameters of 62 ± 3, 79 ± 4, and 103 ± 6 nm, respectively.

Preparation and Characterization of Mechanical Properties of PEDOT:PSS and PS NP-PEDOT:PSS Films. Bending tests were performed on the PEDOT:PSS and PS NP-PEDOT:PSS films by using a universal mechanical test machine (eXpert 4000, ADMET). To prepare the samples, the PS NP solution was added to the PEDOT:PSS solution with different volume fractions, and they were spin coated for 40 s at 2000 rpm on the O_2-plasma treated polyimide (PI) substrate (0.3 cm × 3.1 cm × 0.2 mm), and tests were performed at room temperature at a constant bending radius (γ = 2 mm) for 500 times. As the films were deformed by uniaxial bending, the electrical resistance of the films was characterized with Keithley 2400 and Agilent 34410A multimeter using the four-point probe technique. Field emission scanning electron microscopy (FE-SEM) was performed to determine the size distribution of PS NPs, and observe the surface morphologies of the PS NP-PEDOT:PSS films after the mechanical tests.

Charaterization of PSCs. BHJ-type photovoltaic cells were fabricated using an ITO/ABL/PTB7:$PC_{71}BM$/LiF/Al structure. The photovoltaic performances of the devices were characterized using a solar simulator (Newport Oriel Solar Simulators) with air mass 1.5 G filters. The intensity of the solar simulator was carefully calibrated using an AIST-certified silicon photodiode. The current−voltage behavior was measured using a Keithley 2400 SMU. The active area of the fabricated devices was 0.10 cm^2.

Characterization of Mechanical Properties of PSCs. For the double cantilever beam (DCB) fracture mechanics test, all samples were fabricated using the following procedure. A 25 nm thick Li layer and a 75 nm thick Al layer were deposited on the active layer by a thermal evaporation process. This additional metal thin film structure was employed as a stiff elastic standoff layer in order to prevent plastic deformation of epoxy and associated plastic energy contributions to the adhesion energy of the active layer. Also, they are essential for preventing the permeation of epoxy into the active layer. Afterward, 353nd epoxy (Epo-Tek 353ND consisting of bisphenol F and imidazole; Epoxy Technology) with 1 μm thickness was coated on the Al layer, and dummy glass substrate was attached for making a sandwich structure. The fracture mechanics testing of the DCB specimen was conducted by using a high-precision micromechanical test system (Delaminator Adhesion Test System, DTS Company). Supporting Information Figure

DOI: 10.1021/am507710p
ACS Appl. Mater. Interfaces 2015, 7, 2668−2676

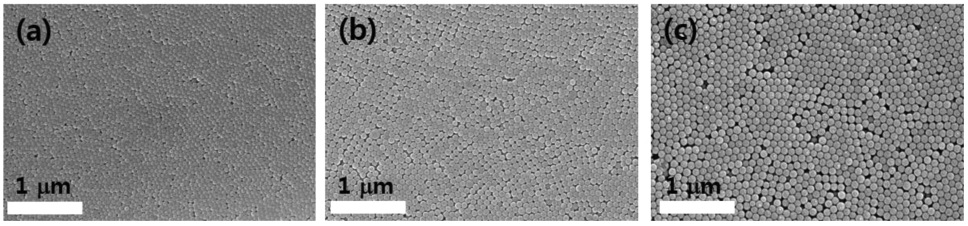

Figure 1. Scanning electron microscopy (SEM) images of three different sizes of PS NPs: (a) 62 ± 3 nm, (b) 79 ± 4 nm, and (c) 103 ± 6 nm. The scale bar is 1 μm.

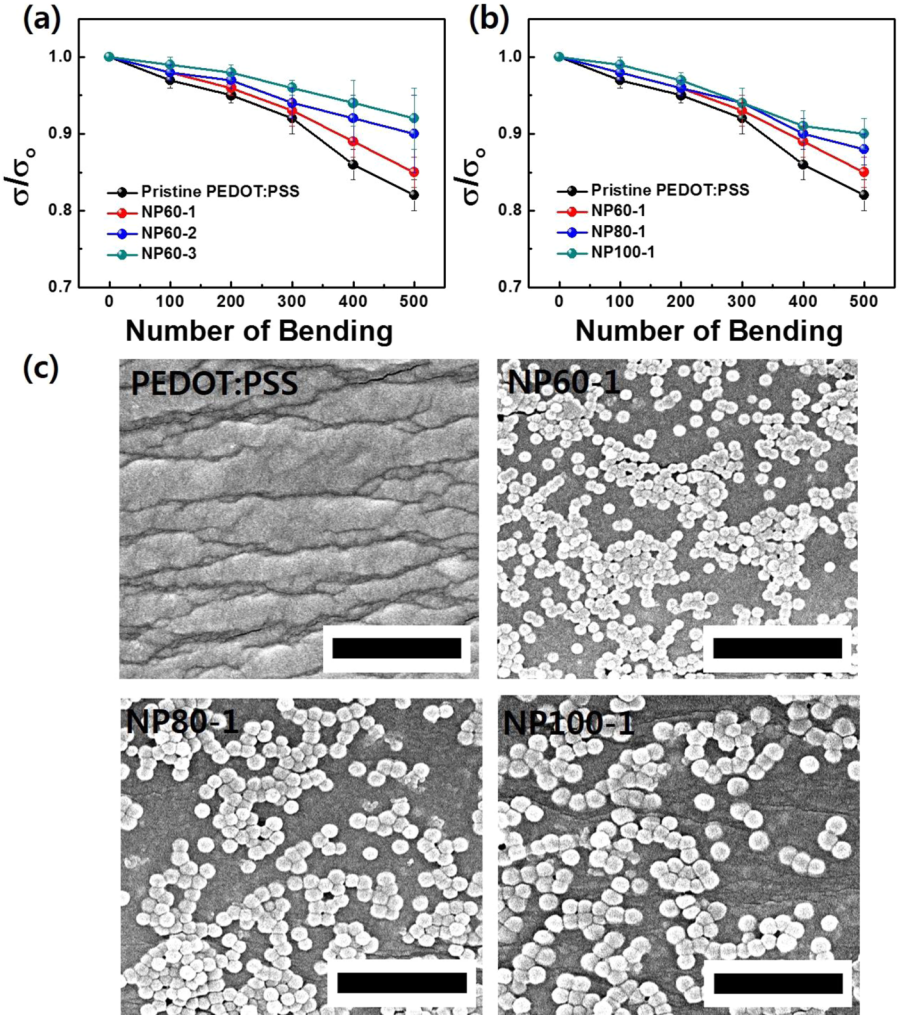

Figure 2. (a) σ/σ_0 values of the pristine PEDOT:PSS, **NP60-1**, **NP60-2**, and **NP60-3** on the PI substrate as a function of bending cycles at constant bending radius (γ = 2 mm). (b) The σ/σ_0 values of the pristine PEDOT:PSS, **NP60-1**, **NP80-1**, and **NP100-1** as a function of the bending cycles. (c) SEM images of pristine PEDOT:PSS and **NP60-1**, **NP80-1**, and **NP100-1** after the 500 bending cycles. The scale bars are 1 μm.

S3(a) also shows the specimen structure for DCB test. The sandwiched thin films between glass substrates were loaded under constant displacement rate of 2 μm s^{-1} while the applied load was continuously monitored as a function of displacement as shown in Supporting Information Figure S3(b). The G_c was calculated by following previous works..[41,42] The Scotch tape peel test was performed using a universal test machine (INSTRON UTM 5940) at 25 °C with a crosshead speed of 50 mm/min, and then the applied load was monitored as a function of displacement.

RESULTS AND DISCUSSION

Preparation of Different Sizes of Cross-Linked PS NPs. Highly monodispersed and cross-linked PS NPs were synthesized via emulsion polymerization as shown in Figure 1. The size of the PS NPs can be controlled by tuning concentrations of the styrene, stabilizer, and DVB as cross-linking agent.[43] We carefully controlled the reaction conditions including nucleation time and concentrations of DVB in order to produce highly monodispersed PS NPs. The higher ratio of styrene monomer to others during the reaction produces the larger size PS NPs. The detailed experimental conditions are described in Supporting Information Table S1. We synthesized a series of three different PS NPs with sizes of 62 ± 3, 79 ± 4, and 103 ± 6 nm, respectively. For convenience, the three different sizes of PS NPs were

DOI: 10.1021/am507710p
ACS Appl. Mater. Interfaces 2015, 7, 2668−2676

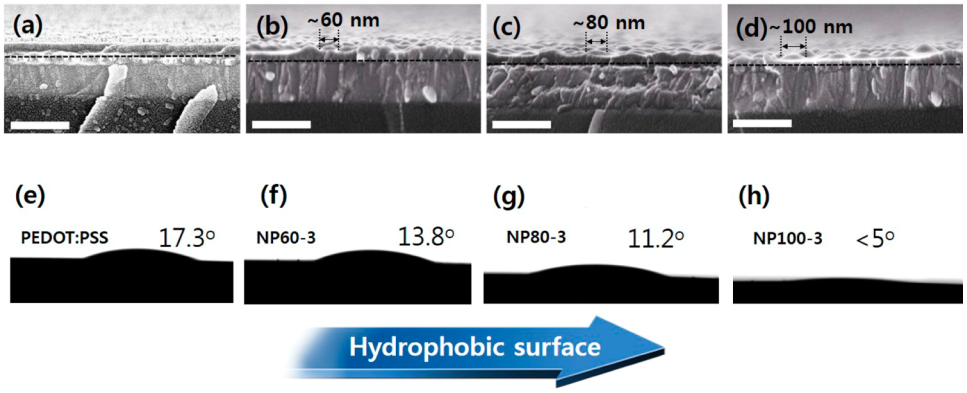

Figure 3. SEM images show the cross-sectional morphologies of the PS NP-PEDOT:PSS/ITO films: (a) pristine PEDOT:PSS, (b) **NP60-3**, (c) **NP80-3**, (d) **NP100-3** films. The images were taken at a tilt angle of 2°. The scale bars are 300 nm. Contact angle measurements. Representative photographic images of diiodomethane droplet on the PS NP-PEDOT:PSS films: (e) pristine PEDOT:PSS, (f) **NP60-3**, (g) **NP80-3**, (h) **NP100-3** films.

denoted as **NP60**, **NP80**, and **NP100**, based on their approximate values.

Preparation and Characterization of PS NP-PEDOT:PSS Films. To control the mechanical and surface properties of the PEDOT:PSS films, we incorporated three different sizes of PS NPs with different ϕ_{NP} into the PEDOT:PSS film (PS NP-PEDOT:PSS). The synthesized PS NPs can be dispersed stably in water, which facilitates the spontaneous fabrication of the PS NP-PEDOT:PSS film by simple one-step fabrication via a spin-coating process. The PS NP-PEDOT:PSS films were prepared on the PI substrate by spin-casting from the mixture of aqueous solutions of PS NP and PEDOT:PSS with different ϕ_{NP} ratios. The ϕ_{NP} value represents the volume fraction of PS NPs to (PS NP + PEDOT:PSS) in the aqueous solution. To estimate the ϕ_{NP} value in each sample, we measured the exact masses of the PS NPs and the PEDOT:PSS before preparing different PS NP-PEDOT:PSS inks. We prepared 9 different PS NP-PEDOT:PSS films that were made from three different sizes of PS NPs and three different ϕ_{NP} values. For convenience, we labeled the PS NP (60 nm size)-PEDOT:PSS films with different ϕ_{NP} values of 0.2, 0.4, and 0.6 as **NP60-1**, **NP60-2**, and **NP60-3**, respectively. Also, the PS NP (80 nm size)-PEDOT:PSS films with different ϕ_{NP} values of 0.2, 0.4, and 0.6 were denoted as **NP80-1**, **NP80-2**, and **NP80-3**, respectively. Similarly, the PS NP (100 nm size)-PEDOT:PSS films with different ϕ_{NP} values of 0.2, 0.4, and 0.6 were denoted as **NP100-1**, **NP100-2**, and **NP100-3**, respectively.

First, to investigate the effect of the PS NPs on the mechanical properties of PS NP-PEDOT:PSS film, we applied a bending stress, which is a simple method for evaluating the fracture toughness of polymers, onto the pristine PEDOT:PSS and PS NP-PEDOT:PSS films. To monitor the effect of the bending stress, we measured the electrical conductivity (σ) of the PS NP-PEDOT:PSS film by four point probe method after applying the bending stress; this measurement was repeated 500 times at a constant bending radius (γ = 2 mm). The initial electrical conductivity (σ_0) values of pristine PEDOT:PSS and all PS NP-PEDOT:PSS were similar in the range 0.9−1.2 S/cm, which agrees well with the previously reported values of the PEDOT:PSS film (Clevios PH500).[22] Also, the addition of PS NP even with large ϕ_{NP} did not affect the intrinsic conductivity of the PEDOT:PSS films because PS NP-PEDOT:PSS films could maintain the percolated conducting pathway through the PEDOT:PSS domain up to ϕ_{NP}= 0.8.[37] Figure 2a shows the variation of normalized electrical conductivity (σ/σ_0) of the pristine PEDOT:PSS, **NP60-1**, **NP60-2**, and **NP60-3** as a function of the number of bending cycles. The σ/σ_0 value of the pristine PEDOT:PSS film decreased rapidly from 1 to 0.8 after 500 times of the bending test, whereas, after applying the same bending stress, the σ/σ_0 values of **NP60-1**, **NP60-2**, and **NP60-3** were decreased to 0.86, 0.92, and 0.94, respectively. These results indicated that higher amount of PS NPs at the given size of the NPs could reduce the crack formations and propagations in the PEDOT:PSS film. In addition, we examined the size effects of PS NPs on the σ/σ_0 values, as shown in Figure 2b. The addition of the larger size PS NPs, i.e., **NP80-1** and **NP100-1**, resulted in relatively higher σ/σ_0 values than **NP60-1** at the same bending test conditions. Thus, the fracture toughness of PS NP-PEDOT:PSS can be enhanced gradually by increasing the ϕ_{NP} values of the PS NPs and their size. These trends can be explained by the findings in the fracture response study using the particle-reinforced polymer composites.[44−46]

For better understanding of the fracture toughness improvements by addition of the PS NPs, we investigated the surface morphologies of the pristine PEDOT:PSS, **NP60-1**, **NP80-1**, and **NP100-1** after applying the 500 bending cycles. As shown in Figure 2c, the surface morphology of the pristine PEDOT:PSS film exhibited numerous cracks and deformations that are commonly observed from brittle polymers.[47] As the cracks in the film were propagated in the direction perpendicular to the bending stress, the electrical conductivity decreased rapidly due to the disconnection between the PEDOT:PSS domains. In contrast to the pristine PEODT:PSS, the **NP60-1**, **NP80-1**, and **NP100-1** had far less pronounced deformations without any crack formation due to the presence of the highly elastic PS NPs in the film.[48]

Next, we compared the surface resistance (R) of the PEDOT:PSS, **NP60-1**, and **NP80-1** films during tensile test at high strain rate (1×10^{-3} s^{-1}) (Supporting Information Figure S1). The normalized resistance (R/R_0) was gradually decreased as the applied tensile strain increased up to 40% because conductive PEDOT within the PEDOT:PSS films was better aligned following the direction of the applied stresses.[49,50] Above the strain of 40%, cracks occurred in the pristine PEDOT:PSS film, and they spread out extensively; eventually the R value increased sharply at 40% strain due to significant crack propagation. In stark contrast, the introduction of PS NPs enhanced the tensile strength of the films, and the R values of the **NP60-1** and **NP80-1** films were stable up to 60% strain. This occurred because the highly elastic characteristics of the PS NPs allowed them to act as binders within the brittle PEDOT:PSS

DOI: 10.1021/am507710p
ACS Appl. Mater. Interfaces 2015, 7, 2668−2676

film.[51] However, we did not observe a strong dependence of the R/R_0 change as a function of the PS NP size, because the PI substrate failed first at approximately 60% strain, which is lower than the critical strain value to produce serious propagation of the cracks in the **NP60-1** and **NP80-1** films. The effect of the PS NPs on the tensile properties of the films was also proven by comparing the surface morphologies of the PEDOT:PSS, **NP60-1**, **NP80-1**, and **NP100-1** films after the tensile stretching tests at 40% strain (Supporting Information Figure S2). The crack phenomenon in PEDOT:PSS was significantly reduced by adding the PS NPs, but we did not observe the distinct difference in the surface morphologies of the **NP60-1**, **NP80-1**, and **NP100-1** films. The results of both bending and tensile experiments consistently supported that the PS NPs can be used successfully as binders to enhance the mechanical stabilities of the PEDOT:PSS film.

In addition to the effect of the PS NPs as binders, they can be used for enhancing the interfacial adhesion between the hydrophilic PEDOT:PSS film and the hydrophobic active layer because the addition of hydrophobic PS NPs into the PEDOT:PSS can alleviate the mismatch of the hydrophobicity between two layers. To examine this effect, first, we investigated the surface properties of the PS NP-PEDOT:PSS films in terms of the sizes and ϕ_{NP} values of the PS NPs. The surface properties were quantified by measuring the static contact angles (CA) of diiodomethane on each different film. Figure 3a–d shows the representative cross-sectional morphologies of pristine PEDOT:PSS, **NP60-3**, **NP80-3**, and **NP100-3**, and Figure 3e–h shows the results of the CA measurements using diiodomethane. The prisitine PEDOT:PSS film had a smooth surface. In contrast, the 60, 80, and 100 nm PS NPs produced a random pattern of corrugated surface on the PS NP-PEDOT:PSS film,[52] because their sizes were larger than the optimum thickness (~50 nm) of the PEDOT:PSS film used in this study. For example, the average depth of the corrugated surface features on the **NP100-3** was determined to be approximately 50 nm, which was in good agreement with the difference between the size of the PS NPs (100 nm) and the thickness of PEDOT:PSS (50 nm). This protruded fraction of the PS NPs on the PEDOT:PSS film increased with the size of the PS NPs, producing the more hydrophobic surface of the PS NP-PEDOT:PSS. In this respect, the CA values of pristine PEDOT:PSS, **NP60-3**, **NP80-3**, and **NP100-3** were remarkably reduced from 17.3°, 13.8°, 11.2°, to less than 5°, respectively. Also, the CA values of the films decreased with the increasing ϕ_{NP} values of PS NP-PEDOT:PSS (i.e., **NP60-1**, 16.2°; **NP60-2**, 15.7°; and **NP60-3**, 13.8°), but the ϕ_{NP} effects on the CA values were much less significant. The hydrophobic characteristics of PS NP-PEDOT:PSS were controllable by changing the PS NP sizes and the ϕ_{NP} values.[53−57] These results indicate that the incorporation of the PS NPs into PEDOT:PSS film can enhance the interfacial interaction between the hydrophilic PEDOT:PSS layer and the hydrophobic active layer.

Application of PS NP-PEDOT:PSS Films for PSCs. To investigate the effects of PS NPs on the performance and long-term stability of the PSCs, bulk heterojuction (BHJ)-type PSC devices that consisted of ITO/pristine PEDOT:PSS or PS NP-PEDOT:PSS ABL/BHJ active layer/LiF/Al were fabricated on the basis of PTB7 as the electron donor and $PC_{71}BM$ as the electron acceptor.[58,59] The active layer of the devices was prepared under the identical conditions including the same blend ratio of PTB7 to $PC_{71}BM$ (1:1.5, w/w) and the same solvent concentration. Also, when fabricating the PSC devices, such as spin-coating the active layer on top of the PS NP-PEDOT:PSS, the cross-linked PS NPs were stable with respect to swelling or dissolution in any organic solvent. Table 1 and Figure 4 show the device characteristics of the PSCs as a function of the ϕ_{NP} values and the sizes of the PS NPs. The control device containing pristine PEDOT:PSS exhibited the PCE value of 7.56%, the open circuit voltage (V_{OC}) of 0.76 V, the short-circuit current (J_{SC}) of 15.42 mA cm^{-2}, and the fill factor (FF) of 0.65. This result was in good agreement with the previously values reported for optimized PTB7-based devices.[58,60,61] Interestingly, all of the devices with PS NP-PEDOT:PSS had comparable performances of approximately 7.5%, irrespective of the PS NP sizes and the ϕ_{NP} values (Figure 4). In particular, the PSC devices with the **NP60-1** and the **NP60-2** had the PCE values of 7.62% and 7.77%, respectively. Therefore, the PS NP-PEDOT:PSS layers

Table 1. Characteristics of the PTB7:$PC_{71}BM$ Based PSC Devices with Different PS NP-PEDOT:PSS ABLs

sample	volume fraction (ϕ_{NP})	V_{OC} (V)	J_{SC} (mA/cm^2)	FF	PCE (%)
reference		0.76	15.42	0.65	7.56
NP60-1	0.2	0.76	16.14	0.62	7.62
NP60-2	0.4	0.76	15.56	0.66	7.77
NP60-3	0.6	0.76	14.60	0.67	7.46
NP80-1	0.2	0.76	15.95	0.62	7.53
NP100-1	0.2	0.76	16.07	0.60	7.40

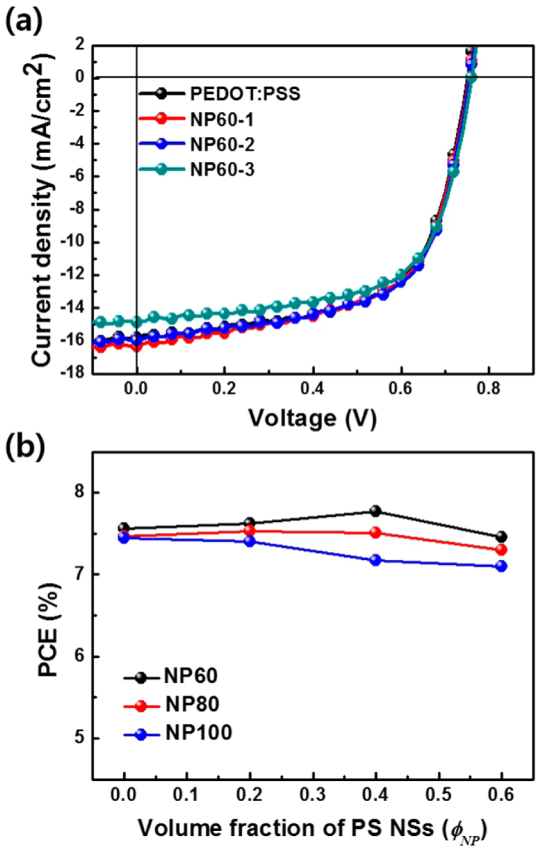

Figure 4. (a) Current density–voltage (J–V) characteristics of PSCs with the pristine PEDOT:PSS, **NP60-1**, **NP60-2**, and **NP60-3** ABLs. (b) Comparison of the PCE values of the PSCs as a function of ϕ_{NP} values for different PS NP sizes. All devices were fabricated and measured under the same condition of AM 1.5 illumination at 100 mW cm^{-2}.

DOI: 10.1021/am507710p
ACS Appl. Mater. Interfaces 2015, 7, 2668–2676

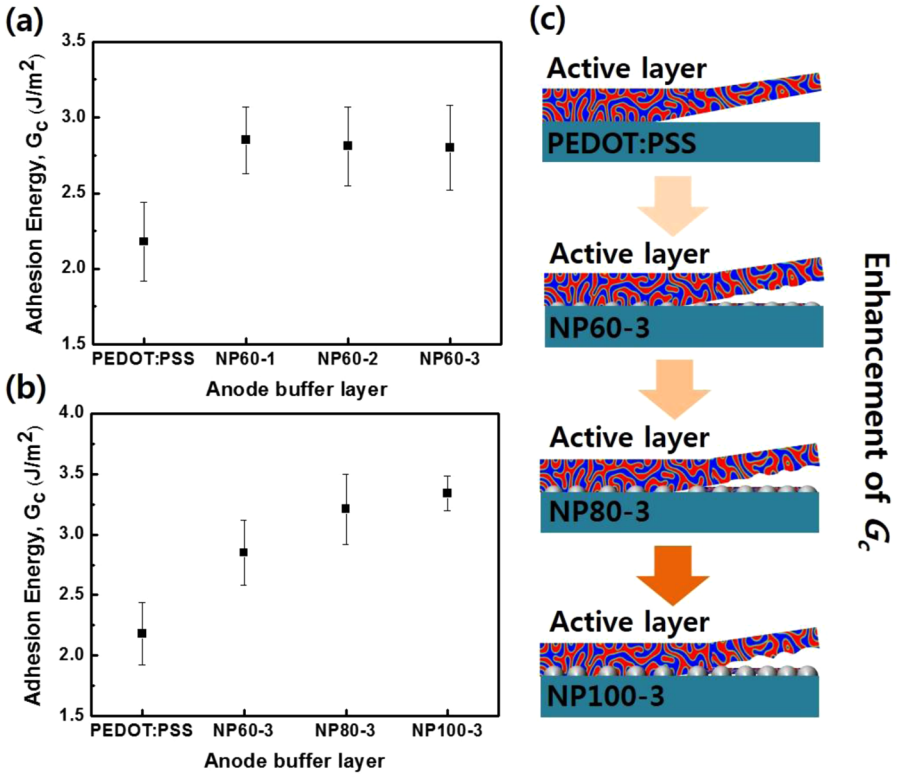

Figure 5. Comparison of adhesion energies (G_c) between the PTB7:$PC_{71}BM$ active layer and the PS NP-PEDOT:PSS film in the actual PSC devices. Part a compares the G_c values of the pristine PEDOT:PSS, **NP60-1**, **NP60-2**, and **NP60-3** ABLs with different ϕ_{NP} values, while part b shows the G_c values of the pristine PEDOT:PSS, **NP60-3**, **NP80-3**, and **NP100-3** for different PS NP sizes. Part c is a schematic illustration of the effect of different sizes of PS NPs on enhancing the G_c values.

can be used successfully in PSCs without any deterioration of the PCE, even for the addition of the largest PS NPs (100 nm). Furthermore, the PS NPs provided the significant advantages of improving the ambient stabilities of the PSCs. We investigated the ambient stabilities of the PSCs with different sizes of PS NPs by comparing the PCE values as a function of the storage time at test conditions (i.e., at room temperature with 45% humidity without encapsulation), as shown in Supporting Information Figure S3. The PCE value of the control device decreased by 97% after the device was exposed to air for 50 h. In contrast, the PSCs with **NP60-3**, **NP80-3**, and **NP100-3** had much greater normalized PCE values of more than 55% for the same conditions. Also, as shown in Supporting Information Figure S4, these features were supported by the thermogravimetric analysis (TGA) and X-ray photoelectron spectroscopy (XPS) measurements, demonstrating that PS NPs effectively suppressed the absorption of moisture by PEDOT:PSS polymers and the indium diffusion to the active layer through the PEDOT:PSS layer.[28,62,63]

Mechanical Properties of PSCs with PS NP-PEDOT:PSS ABLs. In order to examine the effects of PS NP-PEDOT:PSS on the interfacial properties and the mechanical durability of PSCs, we carefully measured G_c between the PS NP-PEDOT:PSS film and the PTB7:$PC_{71}BM$ BHJ active layer, which can be quantified in terms of the macroscopic work of fracture per unit area to separate two layers. We used the DCB fracture mechanics test for measuring the G_c values as functions of the sizes and the ϕ_{NP} values of the PS NPs (Figure 5). The detailed conditions of the DCB test are illustrated in Supporting Information Figure S5.[64,65] First, we compared the G_c values at the interface between the PTB7:$PC_{71}BM$ blend film and the pristine PEDOT:PSS, **NP60-1**, **NP60-2**, and **NP60-3**, respectively. The G_c value was enhanced significantly by adding 60 nm size PS NPs from 2.2 ± 0.3 (pristine PEDOT:PSS) to 2.9 ± 0.2 J/m^2 (**NP60-1**). However, there were not many differences of the G_c values upon increasing ϕ_{NP} values: **NP60-2** (G_c = 2.8 ± 0.3 J/m^2) and **NP60-3** (G_c = 2.8 ± 0.3 J/m^2). Next, the effect of the NP sizes at the same ϕ_{NP} value was investigated by comparing the G_c values of the pristine PEDOT:PSS, **NP60-3**, **NP80-3**, and **NP100-3** (Figure 5b). The G_c values increased remarkably depending on the size of PS NPs (e.g., pristine PEDOT:PSS, 2.2 ± 0.3; **NP60-3**, 2.8 ± 0.3; **NP80-3**, 3.2 ± 0.3; and **NP100-3**, 3.4 ± 0.1 J/m^2). These observations agree well with the changes of the surface properties of the PS NP-PEDOT:PSS films (Figure 3 and Supporting Information Table S2). Whereas the CA values on the PS NP-PEDOT:PSS films did not change significantly with different ϕ_{NP} values, the surface hydrophobicity of the **NP60**, **NP80**, and **NP100** at the same ϕ_{NP} values was increased dramatically. The PS NPs can enhance the resistance against the crack growth and the debonding between the active layer and the PEDOT:PSS and improve their interfacial adhesion, resulting in improved mechanical durability of the PSCs.

To gain a better understanding on the changes of the G_c values with different sizes of the PS NPs, the morphologies of the debonded surfaces of the pristine PEDOT:PSS, **NP60-3**, **NP80-3**, and **NP100-3** were investigated after DCB experiments (Supporting Information Figure S6), which represent the interfacial morphologies between the PS NP-PEDOT:PSS/BHJ active layers. The pristine PEDOT:PSS/BHJ active layer showed a relatively smooth surface due to the low adhsion energy. After the same DCB test, the PS NP-PEDOT:PSS film had a much rougher surface compared to that without the PS

DOI: 10.1021/am507710p
ACS Appl. Mater. Interfaces 2015, 7, 2668−2676

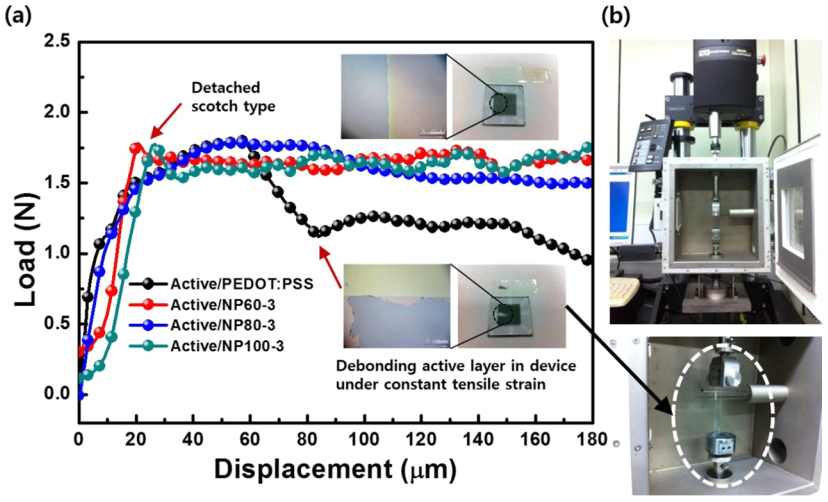

Figure 6. (a) Load–displacement curve for debonding between PS NP-PEDOT:PSS film including pristine PEDOT:PSS, **NP60-3**, **NP80-3**, and **NP100-3**, respectively, and the PTB7:$PC_{71}BM$ active layer. (b) The Scotch tape peel test was measured using a Micro-INSTRON at 25 °C with a crosshead speed of 50 mm/min according to ASTM D412 specifications.

NPs. Also, the surface roughness increased as the size of PS NPs increased. The more hydrophobic surface of the PS NP-PEDOT:PSS was generated with larger size PS NPs, resulting in the stronger interfacial adhesion.

Furthermore, the effect of the PS NPs on the interfacial adhesion of the PSCs can be simply demonstrated by the Scotch tape peel test and directly visualized by the observation of the debonded surfaces after the peel test (Figure 6a). The PTB7:$PC_{71}BM$ blend films were prepared on the pristine PEDOT:PSS, **NP60-3**, **NP80-3**, and **NP100-3**, following the same conditions for the optimized PSCs. The Scotch tape was attached to the top of the active layer, and then, they were peeled off by applying the load of 1.8 N with a constant stretching speed of 50 mm/min (Figure 6b). As shown in Figure 6a, the active layer of the pristine PEDOT:PSS was detached at a lower load (1.3 N) than the applied load (1.8 N) with displacement of 80 μm. In contrast, the PTB7:$PC_{71}BM$ BHJ film on the **NP60-3**, **NP80-3**, and **NP100-3** samples were well-maintained under the 1.8 N load. The inset images of Figure 6a show that the active layer prepared on the pristine PEDOT:PSS was partially detached after the peeling test whereas all of the active layers on the **NP60-3**, **NP80-3**, and **NP100-3** films were intact and undamaged. These results were in excellent agreement with the results of the DCB test, demonstrating that the PS NPs improved the interfacial adhesion between PEDOT:PSS and the active layer.

CONCLUSIONS

Three different sizes of PS NPs were introduced into PEDOT:PSS ABL with different ϕ_{NP} values in order to improve the mechanical and ambient stabilities of PSCs. The PS NP-PEDOT:PSS films were successfully applied in the PTB7:$PC_{71}BM$ based PSCs without any deterioration of their efficiency; all of the devices with 60, 80, and 100 nm PS NPs showed comparable performance of 7.5% but with much enhanced stabilities. The PS NPs acted as not only the binders in the PEDOT:PSS domains, but also the interfacial modifiers between PEDOT:PSS and the active layer in the PSCs. The fracture toughness and tensile strength of the PS NP-PEDOT:PSS films were increased depending on the ϕ_{NP} values and the sizes of PS NPs. Also, the addition of size-tuned PS NPs modified the hydrophobic characteristics of the surface of PS NP-PEDOT:PSS. Therefore, the surface-structured PS NP-PEDOT:PSS films show much improved G_c values between the ABL and active layer in the PSCs, in which the size of the PS NPs had a significant effect on the G_c value. We demonstrated that the use of PS NPs to modify the PEDOT:PSS films is a simple yet powerful route for the fabrication of mechanically robust, air-stable, organic electronic devices.

ASSOCIATED CONTENT

Supporting Information

Synthesis conditions for PS NPs and additional characterization data, including surface resistance, SEM, TGA, XPS, and DCB measurements. This material is available free of charge via the Internet at http://pubs.acs.org.

AUTHOR INFORMATION

Corresponding Author

*E-mail: bumjoonkim@kaist.ac.kr.

Notes

The authors declare no competing financial interest.

ACKNOWLEDGMENTS

This research was supported by the National Research Foundation Grant (2012M1A2A2671746), and by the Global Frontier R&D Program on Center for Multiscale Energy System (2012M3A6A7055540), funded by the Korean Government. This research was supported by the New & Renewable Energy Program of KETEP Grant (20133030000130), funded by the Ministry of Trade, Industry & Energy, Republic of Korea. Authors also acknowledge the KAIST-KUSTAR project and Samsung Display Co. for the financial support.

REFERENCES

(1) Lewis, N. S. Toward Cost-Effective Solar Energy Use. *Science* **2007**, *315*, 798–801.

(2) Zhang, W.; Zhao, B.; He, Z.; Zhao, X.; Wang, H.; Yang, S.; Wu, H.; Cao, Y. High-Efficiency ITO-Free Polymer Solar Cells using Highly Conductive PEDOT:PSS/Surfactant Bilayer Transparent Anodes. *Energy Environ. Sci.* **2013**, *6*, 1956–1964.

DOI: 10.1021/am507710p
ACS Appl. Mater. Interfaces 2015, 7, 2668–2676

(3) Søndergaard, R.; Hösel, M.; Angmo, D.; Larsen-Olsen, T. T.; Krebs, F. C. Roll-to-roll Fabrication of Polymer Solar Cells. *Mater. Today* **2012**, *15*, 36−49.
(4) Cheng, Y.-J.; Yang, S.-H.; Hsu, C.-S. Synthesis of Conjugated Polymers for Organic Solar Cell Applications. *Chem. Rev.* **2009**, *109*, 5868−5923.
(5) Krebs, F. C.; Espinosa, N.; Hösel, M.; Søndergaard, R. R.; Jørgensen, M. 25th Anniversary Article: Rise to Power−OPV-Based Solar Parks. *Adv. Mater.* **2014**, *26*, 29−39.
(6) Zhong, H.; Li, Z.; Deledalle, F.; Fregoso, E. C.; Shahid, M.; Fei, Z.; Nielsen, C. B.; Yaacobi-Gross, N.; Rossbauer, S.; Anthopoulos, T. D.; Durrant, J. R.; Heeney, M. Fused Dithienogermolodithiophene Low Band Gap Polymers for High-Performance Organic Solar Cells without Processing Additives. *J. Am. Chem. Soc.* **2013**, *135*, 2040−2043.
(7) You, J.; Dou, L.; Yoshimura, K.; Kato, T.; Ohya, K.; Moriarty, T.; Emery, K.; Chen, C.-C.; Gao, J.; Li, G.; Yang, Y. A Polymer Tandem Solar Cell with 10.6% Power Conversion Efficiency. *Nat. Commun.* **2013**, *4*, 1446.
(8) Zhang, M.; Guo, X.; Zhang, S.; Hou, J. Synergistic Effect of Fluorination on Molecular Energy Level Modulation in Highly Efficient Photovoltaic Polymers. *Adv. Mater.* **2014**, *26*, 1118−1123.
(9) Ye, L.; Zhang, S.; Zhao, W.; Yao, H.; Hou, J. Highly Efficient 2D-Conjugated Benzodithiophene-Based Photovoltaic Polymer with Linear Alkylthio Side Chain. *Chem. Mater.* **2014**, *26*, 3603−3605.
(10) Cabanetos, C.; El Labban, A.; Bartelt, J. A.; Douglas, J. D.; Mateker, W. R.; Fréchet, J. M. J.; McGehee, M. D.; Beaujuge, P. M. Linear Side Chains in Benzo[1,2-b:4,5-b′]dithiophene−Thieno[3,4-c]pyrrole-4,6-dione Polymers Direct Self-Assembly and Solar Cell Performance. *J. Am. Chem. Soc.* **2013**, *135*, 4656−4659.
(11) Kang, T. E.; Kim, K.-H.; Kim, B. J. Design of Terpolymers as Electron Donors for Highly Efficient Polymer Solar Cells. *J. Mater. Chem. A* **2014**, *2*, 15252−15267.
(12) Nguyen, T. L.; Choi, H.; Ko, S. J.; Uddin, M. A.; Walker, B.; Yum, S.; Jeong, J. E.; Yun, M. H.; Shin, T. J.; Hwang, S.; Kim, J. Y.; Woo, H. Y. Semi-Crystalline Photovoltaic Polymers with Efficiency Exceeding 9% in a [similar]300 nm Thick Conventional Single-Cell Device. *Energy Environ. Sci.* **2014**, *7*, 3040−3051.
(13) Dupont, S. R.; Novoa, F.; Voroshazi, E.; Dauskardt, R. H. Decohesion Kinetics of PEDOT:PSS Conducting Polymer Films. *Adv. Funct. Mater.* **2014**, *24*, 1325−1332.
(14) Bruner, C.; Miller, N. C.; McGehee, M. D.; Dauskardt, R. H. Molecular Intercalation and Cohesion of Organic Bulk Heterojunction Photovoltaic Devices. *Adv. Funct. Mater.* **2013**, *23*, 2863−2871.
(15) Jørgensen, M.; Norrman, K.; Gevorgyan, S. A.; Tromholt, T.; Andreasen, B.; Krebs, F. C. Stability of Polymer Solar Cells. *Adv. Mater.* **2012**, *24*, 580−612.
(16) Jørgensen, M.; Norrman, K.; Krebs, F. C. Stability/Degradation of Polymer Solar Cells. *Sol. Energy Mater. Sol. Cells* **2008**, *92*, 686−714.
(17) Girtan, M.; Rusu, M. Role of ITO and PEDOT:PSS in Stability/Degradation of Polymer:Fullerene Bulk Heterojunctions Solar Cells. *Sol. Energy Mater. Sol. Cells* **2010**, *94*, 446−450.
(18) Kim, H. J.; Kim, J.-H.; Ryu, J.-H.; Kim, Y.; Kang, H.; Lee, W. B.; Kim, T.-S.; Kim, B. J. Architectural Engineering of Rod−Coil Compatibilizers for Producing Mechanically and Thermally Stable Polymer Solar Cells. *ACS Nano* **2014**, *8*, 10461−10470.
(19) Frohne, H.; Shaheen, S. E.; Brabec, C. J.; Müller, D. C.; Sariciftci, N. S.; Meerholz, K. Influence of the Anodic Work Function on the Performance of Organic Solar Cells. *ChemPhysChem* **2002**, *3*, 795−799.
(20) Cho, C.-K.; Hwang, W.-J.; Eun, K.; Choa, S.-H.; Na, S.-I.; Kim, H.-K. Mechanical Flexibility of Transparent PEDOT:PSS Electrodes Prepared by Gravure Printing for Flexible Organic Solar Cells. *Sol. Energy Mater. Sol. Cells* **2011**, *95*, 3269−3275.
(21) Kawano, K.; Pacios, R.; Poplavskyy, D.; Nelson, J.; Bradley, D. D. C.; Durrant, J. R. Degradation of Organic Solar Cells due to Air Exposure. *Sol. Energy Mater. Sol. Cells* **2006**, *90*, 3520−3530.
(22) Oh, J. Y.; Shin, M.; Lee, J. B.; Ahn, J.-H.; Baik, H. K.; Jeong, U. Effect of PEDOT Nanofibril Networks on the Conductivity, Flexibility, and Coatability of PEDOT:PSS Films. *ACS Appl. Mater. Interfaces* **2014**, *6*, 6954−6961.
(23) Brand, V.; Bruner, C.; Dauskardt, R. H. Cohesion and Device Reliability in Organic Bulk Heterojunction Photovoltaic Cells. *Sol. Energy Mater. Sol. Cells* **2012**, *99*, 182−189.
(24) Dong, Q.; Zhou, Y.; Pei, J.; Liu, Z.; Li, Y.; Yao, S.; Zhang, J.; Tian, W. All-Spin-Coating Vacuum-Free Processed Semi-Transparent Inverted Polymer Solar Cells with PEDOT:PSS Anode and PAH-D Interfacial Layer. *Org. Electron.* **2010**, *11*, 1327−1331.
(25) Lee, J. U.; Jung, J. W.; Jo, J. W.; Jo, W. H. Degradation and Stability of Polymer-based Solar Cells. *J. Mater. Chem.* **2012**, *22*, 24265−24283.
(26) Dupont, S. R.; Voroshazi, E.; Nordlund, D.; Vandewal, K.; Dauskardt, R. H. Controlling Interdiffusion, Interfacial Composition, and Adhesion in Polymer Solar Cells. *Adv. Mater. Interfaces* **2014**, *1*, 1400135.
(27) Dupont, S. R.; Voroshazi, E.; Heremans, P.; Dauskardt, R. H. Adhesion Properties of Inverted Polymer Solarcells: Processing and Film Structure Parameters. *Org. Electron.* **2013**, *14*, 1262−1270.
(28) de Jong, M. P.; van Ijzendoorn, L. J.; de Voigt, M. J. A. Stability of the Interface between Indium-Tin-Oxide and Poly(3,4-ethylenedioxythiophene)/Poly(styrenesulfonate) in Polymer Light-Emitting Diodes. *Appl. Phys. Lett.* **2000**, *77*, 2255−2257.
(29) Wong, K. W.; Yip, H. L.; Luo, Y.; Wong, K. Y.; Lau, W. M.; Low, K. H.; Chow, H. F.; Gao, Z. Q.; Yeung, W. L.; Chang, C. C. Blocking Reactions between Indium-Tin Oxide and Poly(3,4-ethylene dioxythiophene): Poly(styrene sulphonate) with a Self-Assembly Monolayer. *Appl. Phys. Lett.* **2002**, *80*, 2788−2790.
(30) Nardes, A. M.; Kemerink, M.; de Kok, M. M.; Vinken, E.; Maturova, K.; Janssen, R. A. J. Conductivity, Work Function, and Environmental Stability of PEDOT:PSS Thin Films Treated with Sorbitol. *Org. Electron.* **2008**, *9*, 727−734.
(31) Huang, J.; Miller, P. F.; Wilson, J. S.; de Mello, A. J.; de Mello, J. C.; Bradley, D. D. C. Investigation of the Effects of Doping and Post-Deposition Treatments on the Conductivity, Morphology, and Work Function of Poly(3,4-ethylenedioxythiophene)/Poly(styrene sulfonate) Films. *Adv. Funct. Mater.* **2005**, *15*, 290−296.
(32) Yip, H.-L.; Hau, S. K.; Baek, N. S.; Ma, H.; Jen, A. K. Y. Polymer Solar Cells That Use Self-Assembled-Monolayer- Modified ZnO/Metals as Cathodes. *Adv. Mater.* **2008**, *20*, 2376−2382.
(33) Hau, S. K.; Yip, H.-L.; Acton, O.; Baek, N. S.; Ma, H.; Jen, A. K. Y. Interfacial Modification to Improve Inverted Polymer Solar Cells. *J. Mater. Chem.* **2008**, *18*, 5113−5119.
(34) Hau, S. K.; Yip, H.-L.; Ma, H.; Jen, A. K.-Y. High Performance Ambient Processed Inverted Polymer Solar Cells through Interfacial Modification with a Fullerene Self-Assembled Monolayer. *Appl. Phys. Lett.* **2008**, *93*, 233304.
(35) Vosgueritchian, M.; Lipomi, D. J.; Bao, Z. Highly Conductive and Transparent PEDOT:PSS Films with a Fluorosurfactant for Stretchable and Flexible Transparent Electrodes. *Adv. Funct. Mater.* **2012**, *22*, 421−428.
(36) Chen, M.-C.; Chiou, Y.-S.; Chiu, J.-M.; Tedla, A.; Tai, Y. Marked Improvement in the Stability of Small Molecule Organic Photovoltaics by Interfacial Modification using Self-Assembled Monolayers to Prevent Indium Diffusion into the Active Layer. *J. Mater. Chem. A* **2013**, *1*, 3680−3687.
(37) Kang, D. J.; Kang, H.; Kim, K.-H.; Kim, B. J. Nanosphere Templated Continuous PEDOT:PSS Films with Low Percolation Threshold for Application in Efficient Polymer Solar Cells. *ACS Nano* **2012**, *6*, 7902−7909.
(38) Kaltenbrunner, M.; White, M. S.; Glowacki, E. D.; Sekitani, T.; Someya, T.; Sariciftci, N. S.; Bauer, S. Ultrathin and Lightweight Organic Solar Cells with High Flexibility. *Nat. Commun.* **2012**, *3*, 770.
(39) Mengistie, D. A.; Ibrahem, M. A.; Wang, P.-C.; Chu, C.-W. Highly Conductive PEDOT:PSS Treated with Formic Acid for ITO-Free Polymer Solar Cells. *ACS Appl. Mater. Interfaces* **2014**, *6*, 2292−2299.
(40) Alemu, D.; Wei, H.-Y.; Ho, K.-C.; Chu, C.-W. Highly Conductive PEDOT:PSS Electrode by Simple Film Treatment with Methanol for ITO-Free Polymer Solar Cells. *Sol. Energy Mater. Sol. Cells* **2012**, *5*, 9662−9671.
(41) Kim, T.-S.; Tsuji, N.; Matsushita, K.; Kobayashi, N.; Chumakov, D.; Geisler, H.; Zschech, E.; Dauskardt, R. H. Tuning Depth Profiles of

DOI: 10.1021/am507710p
ACS Appl. Mater. Interfaces 2015, 7, 2668−2676

Organosilicate Films with Ultraviolet Curing. *J. Appl. Phys.* **2008**, *104*, 074113.
(42) Hohlfelder, R. J.; Maidenberg, D. A.; Dauskardt, R. H.; Wei, Y.; Hutchinson, W. Adhesion of Benzocyclobutene-Passivated Silicon in Epoxy Layered Structures. *J. Mater. Res.* **2001**, *16*, 243−255.
(43) Choi, J.; Kwak, S. Y.; Kang, S.; Lee, S. S.; Park, M.; Lim, S.; Kim, J.; Choe, C. R.; Hong, S. I. Synthesis of Highly Crosslinked Monodisperse Polymer Particles: Effect of Reaction Parameters on the Size and Size distribution. *J. Polym. Sci., Part A: Polym. Chem.* **2002**, *40*, 4368−4377.
(44) Adachi, T.; Osaki, M.; Araki, W.; Kwon, S.-C. Fracture Toughness of Nano- and Micro-Spherical Silica-Particle-Filled Epoxy Composites. *Acta. Mater.* **2008**, *56*, 2101−2109.
(45) Fu, S.-Y.; Feng, X.-Q.; Lauke, B.; Mai, Y.-W. Effects of Particle size, Particle/Matrix Interface Adhesion and Particle Loading on Mechanical Properties of Particulate−Polymer Composites. *Composites, Part B* **2008**, *39*, 933−961.
(46) Lauke, B. On the Effect of Particle Size on Fracture Toughness of Polymer Composites. *Compos. Sci. Technol.* **2008**, *68*, 3365−3372.
(47) Lang, U.; Müller, E.; Naujoks, N.; Dual, J. Microscopical Investigations of PEDOT:PSS Thin Films. *Adv. Funct. Mater.* **2009**, *19*, 1215−1220.
(48) Cha, Y.-J.; Choe, S. Characterization of Crosslinked Polystyrene Beads and Their Composite in SBR Matrix. *J. Appl. Polym. Sci.* **1995**, *58*, 147−157.
(49) Jalili, R.; Razal, J. M.; Innis, P. C.; Wallace, G. G. One-Step Wet-Spinning Process of Poly(3,4-ethylenedioxythiophene):Poly-(styrenesulfonate) Fibers and the Origin of Higher Electrical Conductivity. *Adv. Funct. Mater.* **2011**, *21*, 3363−3370.
(50) Lee, Y.-Y.; Lee, J.-H.; Cho, J.-Y.; Kim, N.-R.; Nam, D.-H.; Choi, I.-S.; Nam, K. T.; Joo, Y.-C. Stretching-Induced Growth of PEDOT-Rich Cores: A New Mechanism for Strain-Dependent Resistivity Change in PEDOT:PSS Films. *Adv. Funct. Mater.* **2013**, *23*, 4020−4027.
(51) Ji, X. L.; Jing, J. K.; Jiang, W.; Jiang, B. Z. Tensile Modulus of Polymer Nanocomposites. *Polym. Eng. Sci.* **2002**, *42*, 983−993.
(52) Kang, D. J.; Kang, H.; Cho, C.; Kim, K.-H.; Jeong, S.; Lee, J.-Y.; Kim, B. J. Efficient Light Trapping in Inverted Polymer Solar Cells by a Randomly Nanostructured Electrode using Monodispersed Polymer Nanoparticles. *Nanoscale* **2013**, *5*, 1858−1863.
(53) van der Wal, P.; Steiner, U. Super-hydrophobic Surfaces Made from Teflon. *Soft Matter* **2007**, *3*, 426−429.
(54) Owens, D. K.; Wendt, R. C. Estimation of the Surface Free Energy of Polymers. *J. Appl. Polym. Sci.* **1969**, *13*, 1741−1747.
(55) Nakajima, A. Design of Hydrophobic Surfaces for Liquid Droplet Control. *NPG Asia Mater.* **2011**, *3*, 49−56.
(56) Yan, L.; Wang, K.; Wu, J.; Ye, L. Hydrophobicity of Model Surfaces with Loosely Packed Polystyrene Spheres after Plasma Etching. *J. Phys. Chem. B* **2006**, *110*, 11241−11246.
(57) Yang, Q.; Chen, J.; Xu, Q.; He, L.; Chen, Z.; Fu, J. Spherical Assembled Microstructures: Fabrication and Their Stabilization with Assistance of Supercritical Carbon Dioxide. *Soft Matter* **2011**, *7*, 5353−5359.
(58) Liang, Y.; Xu, Z.; Xia, J.; Tsai, S.-T.; Wu, Y.; Li, G.; Ray, C.; Yu, L. For the Bright Future—Bulk Heterojunction Polymer Solar Cells with Power Conversion Efficiency of 7.4%. *Adv. Mater.* **2010**, *22*, E135−E138.
(59) Collins, B. A.; Li, Z.; Tumbleston, J. R.; Gann, E.; McNeill, C. R.; Ade, H. Absolute Measurement of Domain Composition and Nanoscale Size Distribution Explains Performance in PTB7:PC71BM Solar Cells. *Adv. Energy. Mater.* **2013**, *3*, 65−74.
(60) He, Z.; Zhong, C.; Huang, X.; Wong, W.-Y.; Wu, H.; Chen, L.; Su, S.; Cao, Y. Simultaneous Enhancement of Open-Circuit Voltage, Short-Circuit Current Density, and Fill Factor in Polymer Solar Cells. *Adv. Mater.* **2011**, *23*, 4636−4643.
(61) Son, H. J.; Wang, W.; Xu, T.; Liang, Y.; Wu, Y.; Li, G.; Yu, L. Synthesis of Fluorinated Polythienothiophene-co-Benzodithiophenes and Effect of Fluorination on the Photovoltaic Properties. *J. Am. Chem. Soc.* **2011**, *133*, 1885−1894.
(62) Kim, T.; Kang, H.; Jeong, S.; Kang, D. J.; Lee, C.; Lee, C.-H.; Seo, M.-K.; Lee, J.-Y.; Kim, B. J. Au@Polymer Core-Shell Nanoparticles for Simultaneously Enhancing Efficiency and Ambient Stability of Organic Optoelectronic Devices. *ACS Appl. Mater. Interfaces* **2014**, *6*, 16956−16965.
(63) Reese, M. O.; Morfa, A. J.; White, M. S.; Kopidakis, N.; Shaheen, S. E.; Rumbles, G.; Ginley, D. S. Pathways for the Degradation of Organic Photovoltaic P3HT:PCBM based Devices. *Sol. Energy Mater. Sol. Cells* **2008**, *92*, 746−752.
(64) Kim, S.; Pang, I.; Lee, J. Aminosilane SAM-Assisted Patterning of Poly(3,4-ethylenedioxythiophene) Nanofilm Robustly Adhered to SiO2 Substrate. *Macromol. Rapid Commun.* **2007**, *28*, 1574−1580.
(65) Jiang, W.; Zhitenev, N.; Bao, Z.; Meng, H.; Abusch-Magder, D.; Tennant, D.; Garfunkel, E. Structure and Bonding Issues at the Interface between Gold and Self-Assembled Conjugated Dithiol Monolayers. *Langmuir* **2005**, *21*, 8751−8757.

DOI: 10.1021/am507710p
ACS Appl. Mater. Interfaces 2015, 7, 2668−2676